



# PCCP

**Insights into how the aqueous environment influences the kinetics and mechanisms of heterogeneously-catalyzed COH\* and CH<sub>3</sub>OH\* dehydrogenation reactions on Pt(111)**

Journal:	<i>Physical Chemistry Chemical Physics</i>
Manuscript ID	CP-ART-02-2019-000824.R1
Article Type:	Paper
Date Submitted by the Author:	19-Mar-2019
Complete List of Authors:	Bodenschatz, Cameron; Clemson University, Chemical and Biomolecular Engineering Xie, Tianjun; Clemson University, Chemical and Biomolecular Engineering Zhang, Xiaohong; Clemson University Department of Bioengineering, Getman, Rachel; Clemson University, Chemical and Biomolecular Engineering

SCHOLARONE™  
Manuscripts

Cite this: DOI: 10.1039/xxxxxxxxxx

# Insights into how the aqueous environment influences the kinetics and mechanisms of heterogeneously-catalyzed COH\* and CH<sub>3</sub>OH\* dehydrogenation reactions on Pt(111)<sup>†</sup>

Cameron J. Bodenschatz, Tianjun Xie,<sup>‡</sup> Xiaohong Zhang,<sup>‡</sup> and Rachel B. Getman\*

Received Date

Accepted Date

DOI: 10.1039/xxxxxxxxxx

www.rsc.org/journalname

Water influences catalytic reactions in multiple ways, including energetic and mechanistic effects. While simulations have provided significant insight into the roles that H<sub>2</sub>O structures play in aqueous-phase heterogeneous catalysis, questions still remain as to the extent to which they influence catalytic mechanisms. Specifically, influences of the configurational variability in the water structures at the catalyst interface are yet to be understood. Configurational variability is challenging to capture, as it requires multiscale approaches. Herein, we apply a multiscale sampling approach to calculate reaction thermodynamics and kinetics for COH\* dehydrogenation to CO\* and CH<sub>3</sub>OH\* dehydrogenation to CH<sub>2</sub>OH\* on Pt(111) catalysts under liquid H<sub>2</sub>O. We explore various pathways for these dehydrogenation reactions that could influence the overall mechanism of methanol decomposition by including participation of H<sub>2</sub>O structures both energetically and mechanistically. We find that the liquid H<sub>2</sub>O environment significantly influences the mechanism of COH\* dehydrogenation to CO\* but leaves the mechanism of CH<sub>3</sub>OH\* dehydrogenation to CH<sub>2</sub>OH\* largely unaltered.

## 1 Introduction

One of the grand challenges in catalysis research is understanding catalytic mechanisms. This is important since a molecular level understanding of catalytic chemistry can facilitate catalyst selection and design.<sup>1,2</sup> We are specifically interested in reactions that occur under aqueous phase. Examples of applications utilizing aqueous-phase conditions include aqueous-phase processing of biomass,<sup>3–6</sup> alcohol and acid fuel cells,<sup>7–12</sup> wastewater treatment,<sup>13–17</sup> and production of fine chemicals<sup>3,18</sup> and fuels.<sup>18–20</sup> Further, interest in using water as a “green” solvent in catalysis<sup>21</sup> motivates the need to understand how H<sub>2</sub>O molecules influence catalytic chemistry.

Two of the primary ways in which water molecules influence catalytic mechanisms are altering the energies of catalytic species and participating in catalytic reactions. For example, water molecules interact with various chemical species

adsorbed on solid catalyst surfaces through hydrogen bonding and van der Waals interactions.<sup>22–41</sup> These interactions have been shown to depend on the specific catalytic species and thus to influence reaction energies and activation barriers compared to gas phase. In some cases, they have been shown to depend on the specific arrangement of water molecules at the catalyst interface.<sup>23,24,27,42–48</sup> If significant enough, catalytic species interactions with liquid H<sub>2</sub>O can alter dominant reaction pathways compared to gas phase.<sup>24,31,41–43,49</sup> Water can also participate in the reactions themselves. For example, water molecules can act as a source for surface hydrogen atoms and hydroxyl groups.<sup>19,20,28,31,43,50</sup> Further, H<sub>2</sub>O molecules can mediate catalytic reactions, e.g., by promoting cleavage of O–H bonds.<sup>19,20,25–28,30–32,38,39,43,45,47,48,51–59</sup>

While simulations have provided significant insight into the roles that H<sub>2</sub>O molecules play in aqueous-phase heterogeneous catalysis, questions still remain as to the extent to which they influence catalytic mechanisms. One challenge is to properly sample the configurations (i.e., the spatial arrangements) of the liquid H<sub>2</sub>O molecules at the catalyst interface. Configurational variability arises due to temperature, and thus capturing it requires methods beyond quantum mechanics. *Ab initio* molecular dynamics (AIMD) addresses the finite temperature movements of liquid molecules; however, it is computationally intensive and thus lim-

Department of Chemical and Biomolecular Engineering, Clemson University, Clemson, South Carolina 29634, USA. E-mail: rgetman@clemson.edu

<sup>‡</sup> These authors contributed equally to this work.

<sup>†</sup> Electronic Supplementary Information (ESI) available: Calculation details for DFT and MD simulations including force field parameters, geometric criteria for hydrogen bonds and pre-exponential factor calculations, a comparison of implicit and explicit solvation results, structures of H<sub>5</sub>O<sub>2</sub> and H<sub>2</sub>O selected from an AIMD trajectory, and converged TS structures. See DOI: 10.1039/cXCP00000x/

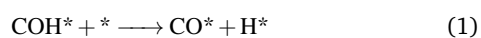
ited in the number of configurations that can be generated.<sup>56,60</sup> Classical molecular dynamics (cMD) can generate liquid water configurations in a more computationally tractable manner but cannot be used to model the breaking and forming of chemical bonds. Alternatively, reactive force fields can capture bond breaking and forming;<sup>61–63</sup> however, reactive force fields are available for a limited number of heterogeneously catalyzed systems. Capturing the influence of configurational variability on catalytic energetics (reaction energies, activation energies) thus requires combining methods that can capture sufficient numbers of configurations as well as the energetics bond breaking and forming. Calculating rate constants for catalytic reactions in liquid H<sub>2</sub>O also requires new methods,<sup>64</sup> as present methods rely on theories based on the assumption that the reaction environment is an ideal gas<sup>43</sup> (and thus are independent of the configuration of fluid phase molecules at the catalyst interface).

Our goal in this work is to improve insight about how the configurational variability of the liquid structure influences catalytic mechanisms. We are specifically interested in comparing reactions involving polar versus non-polar reaction intermediates, which we expect to exhibit different behaviors in water. To explore such phenomena, we model Pt(111)-catalyzed hydroxymethylidyne dehydrogenation to carbon monoxide, i.e.,  $\text{COH}^* + * \longrightarrow \text{CO}^* + \text{H}^*$ , and methanol dehydrogenation to hydroxymethyl, i.e.,  $\text{CH}_3\text{OH}^* + * \longrightarrow \text{CH}_2\text{OH}^* + \text{H}^*$ . These reactions were chosen because they allow comparison of catalytic O–H versus C–H cleavage, which serve as examples for H<sub>2</sub>O participation with hydrophilic versus hydrophobic functional groups, and because they are expected to be part of the dominant reaction pathway in methanol decomposition.<sup>65</sup> To capture the configurational variability, we combine cMD with density functional theory (DFT), in an approach that we recently coined “multiscale sampling.”<sup>60</sup> This method enables the generation of realistic liquid water structures for calculating catalytic quantities. These types of calculations are not possible with DFT or MD by themselves. We use the multiscale sampling approach to calculate reaction energies, activation barriers, and pre-exponential factors for the COH\* and CH<sub>3</sub>OH\* dehydrogenation reactions. Comparing the results for the analogous reactions under vacuum, we provide the most conclusive results to date of the roles of liquid H<sub>2</sub>O molecules on the reaction energies, activation barriers, and pre-exponential factors involved in the COH\* and CH<sub>3</sub>OH\* dehydrogenation reactions on Pt(111). Our results show that the liquid H<sub>2</sub>O environment significantly influences the thermodynamics and kinetics of COH\* dehydrogenation but have a much more minor influence on the thermodynamics and kinetics of CH<sub>3</sub>OH\* dehydrogenation.

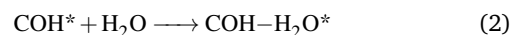
## 2 Methods

### 2.1 Reaction pathways

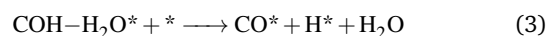
The catalytic dehydrogenations of COH\* and CH<sub>3</sub>OH\* were modeled in three different pathways. The first is “direct” dehydrogenation, where the H atom is transferred directly from the reactant to the catalyst surface, e.g.,



where the \* indicates a vacant binding site on the Pt(111) surface and \*ed species are bound to the catalyst surface. The second and third pathways involve liquid H<sub>2</sub>O molecules and thus require a model for such. While prior literature has shown that at low temperature (< 145 K), H<sub>2</sub>O molecules arrange in hexagonal, ice-like patterns on metal surfaces,<sup>66–69</sup> it is not well-understood how liquid H<sub>2</sub>O molecules adsorb to metal surfaces. Competition between hydrogen bonding, interactions with the metal surface atoms, and thermal fluctuations complicate experimental and computational attempts to visualize a H<sub>2</sub>O molecule reaction intermediate. In our MD simulations (including cMD and AIMD), we have observed that H<sub>2</sub>O molecules near the Pt surface that are not hydrogen bonded to catalytic species remain more fluid-like than the chemically adsorbed reaction intermediates and transition states. That is, H<sub>2</sub>O molecules near the surface demonstrate more significant thermal fluctuations in their spatial positions. Hence, we treat such H<sub>2</sub>O molecules as fluid phase species (i.e., that do not participate in the site balances) in the chemical equations presented below. To participate in a chemical reaction, we assume that a liquid H<sub>2</sub>O molecule near the Pt surface first forms a complex with a reaction intermediate. In these complexation reactions, a near-surface H<sub>2</sub>O molecule interacts with a catalytic species through van der Waal’s interactions and/or hydrogen-bonding, and this interaction lasts for a specified amount of time (i.e., the interaction is not fleeting). The specific requirements are elaborated in Section 2.3. For example, the complexation of COH\* with a liquid H<sub>2</sub>O molecule near the Pt surface is written as



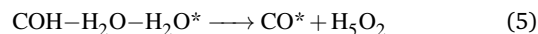
In a subsequent step, the complexed H<sub>2</sub>O molecule can either “co-catalyze” the dehydrogenation,<sup>45,57,70</sup> e.g.,



or “assist” the dehydrogenation. We model the assisted pathway as involving complexation of a second water molecule, e.g.,

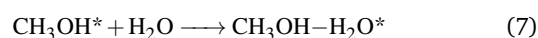


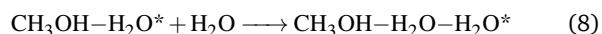
followed by cleavage of the C–H or O–H bond to form H<sub>5</sub>O<sub>2</sub>, e.g.,



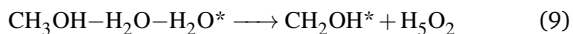
Here, we use the H<sub>5</sub>O<sub>2</sub> species as a general model of H<sub>2n+1</sub>O<sub>n</sub> species. Values of *n* have been shown to vary from 1<sup>30,39,70–72</sup> to 6,<sup>73</sup> depending on the system. We chose H<sub>5</sub>O<sub>2</sub> as a model for H<sub>2n+1</sub>O<sub>n</sub> species since our test calculations show that reaction energetics involving H<sub>2n+1</sub>O<sub>n</sub> species are reasonably converged when *n* = 2. More details about these tests are provided in Section S11 of the ESI†.

Analogous reactions for dehydrogenation of methanol to hydroxymethyl are

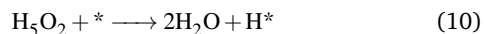




and



respectively, with the exception that we neglected the co-catalyzed pathway because its pre-exponential factor is prohibitively small (see Section 3.4). To complete the  $\text{H}_2\text{O}$ -assisted pathways for both the  $\text{CH}_3\text{OH}^*$  and  $\text{COH}^*$  reactants, we also modeled  $\text{H}_5\text{O}_2$  dehydrogenation, i.e.,



Over the course of the catalytic cycle, a H species is abstracted from a reaction intermediate and deposited on the Pt(111) surface. We generally refer to these species as “hydrogen atoms” in this work; however, we note that these species could alternately be protons.

## 2.2 Reaction energies and activation energies

Aqueous phase reaction energies were calculated as in prior work,<sup>42,43</sup> i.e.:

$$\Delta E_{\text{rxn}}^{\text{aq}} = \Delta E_{\text{rxn}}^{\text{vac}} + \Delta \Delta E_{\text{int}} \quad (11)$$

where  $\Delta E_{\text{rxn}}^{\text{aq}}$  is the reaction energy calculated under liquid water,  $\Delta E_{\text{rxn}}^{\text{vac}}$  is the reaction energy calculated under vacuum, and  $\Delta \Delta E_{\text{int}}$  is the difference in the calculated water-adsorbate interaction energy between products and reactants. For example,  $\Delta E_{\text{rxn}}^{\text{vac}}$  for reaction (1) is calculated as  $\Delta E_{\text{rxn}}^{\text{vac}} = E^{\text{vac}}(\text{CO}^*) + E^{\text{vac}}(\text{H}^*) - E^{\text{vac}}(\text{COH}^*) - E^{\text{vac}}(^*)$ , and  $\Delta E_{\text{int}}$  for  $\text{COH}^*$  is calculated as  $\Delta E_{\text{int}}(\text{COH}^*) = E^{\text{aq}}(\text{COH}^*) + E^{\text{vac}}(^*) - E^{\text{vac}}(\text{COH}^*) - E^{\text{aq}}(^*)$ .<sup>23</sup>  $\Delta E_{\text{int}}$  are reported as averages over 10 configurations of liquid  $\text{H}_2\text{O}$  molecules generated using the cMD-DFT approach, plus or minus the 95% confidence interval. More details about the cMD-DFT method are included in Section S6 of the ESI†.  $\Delta \Delta E_{\text{int}}$  is then calculated by subtracting the interaction energies of the reactants from those of the products, e.g.,  $\Delta \Delta E_{\text{int}} = \Delta E_{\text{int}}(\text{CO}^*) + \Delta E_{\text{int}}(\text{H}^*) - \Delta E_{\text{int}}(\text{COH}^*) - \Delta E_{\text{int}}(^*)$ . Activation energies were calculated analogously,<sup>43</sup> i.e.,

$$\Delta E_{\text{act}}^{\text{aq}} = \Delta E_{\text{act}}^{\text{vac}} + \Delta \Delta E_{\text{int}} \quad (12)$$

where  $\Delta \Delta E_{\text{int}}$  in this case is calculated by subtracting the interaction energy of the reactants from that of the transition state.  $\Delta E_{\text{act}}^{\text{aq}}$  for complexation reactions (2), (4), (7), and (8) were assumed to be low (below  $k_B T$ ) because they do not involve rearrangements of chemical bonds, and thus we set them equal to zero in this work.

## 2.3 Pre-exponential terms

Pre-exponential factors for reactions (1), (3), (5), (6), and (9), which all involve O—H or C—H bond breaking, were approximated as equal to  $k_B T/h$ , where  $k_B$  is Boltzmann’s constant and  $h$  is Planck’s constant.

Reactions (2) and (7) involve complexation of a  $\text{H}_2\text{O}$  molecule with a catalytic species. To help discern the influence of configurational variability in the  $\text{H}_2\text{O}$  structure on the kinetics of these reactions, we estimated their pre-exponential factors from cMD

trajectories as the number of occurrences per unit time that the  $\text{H}_2\text{O}$  structure 1) oriented in a way so as to promote the complexation and 2) held for 0.16 ps using the structural criteria presented below. This procedure was inspired by the work of Savara and coworkers.<sup>64</sup> The time requirement of 0.16 ps is equal to  $h/k_B T$  at the simulation temperature of 300 K, which is approximately equal to the period of a molecular vibration at that temperature. If the  $\text{H}_2\text{O}$  structure held for more than 0.16 ps, then it was counted toward the pre-exponential factor in 0.16 ps increments until it was deemed that it could no longer promote the complexation reaction of interest. In this strategy, a  $\text{H}_2\text{O}$  structure that could continuously promote complexation of a  $\text{H}_2\text{O}$  molecule and a  $\text{COH}^*$  or  $\text{CH}_3\text{OH}^*$  species would have a pre-exponential factor equal to  $k_B T/h$ . A water structure was deemed able to promote a complexation reaction when the distance between the O atom on one of the liquid  $\text{H}_2\text{O}$  molecules and the O or C atom in the relevant —OH or —CH functional group was  $\leq 3.5 \text{ \AA}$  and the corresponding  $\text{O}_{\text{H}_2\text{O}}-\text{O}-\text{H}$  or  $\text{O}_{\text{H}_2\text{O}}-\text{C}-\text{H}$  angle was  $\leq 30^\circ$ . These criteria were adopted from the established geometrical criteria for hydrogen-bonding (see Section S2 of the ESI†).<sup>74,75</sup> However, they only identify the frequency at which reactant- $\text{H}_2\text{O}$  complexes form. To further distinguish  $\text{H}_2\text{O}$  complexes that could promote co-catalyzed dehydrogenation reactions (which represent a fraction of the total), we included two more criteria involving the orientation of the specific  $\text{H}_2\text{O}$  molecule that complexed with the reactant molecule. Specifically, to co-catalyze a dehydrogenation reaction, the  $\text{H}_2\text{O}$  molecule in the complex must comprise a “dangling” hydrogen atom,<sup>56</sup> i.e., which points toward the Pt(111) surface. To capture these specific configurations, we counted structures where the  $c$  coordinate of an H atom from the  $\text{H}_2\text{O}$  molecule was below the  $c$  coordinate of the water O atom and where the distance in the  $c$  dimension between this H atom and the Pt surface plane was  $\leq 2.5 \text{ \AA}$ . These criteria are illustrated in Figure S2 in the ESI†. The pre-exponential factors estimated from structural criteria are presented as averages over at least 5 cMD trajectories, plus or minus the 95% confidence intervals.

Reactions (4) and (8) involve complexation of a second  $\text{H}_2\text{O}$  molecule to a reactant- $\text{H}_2\text{O}$  complex. Since in our cMD simulations liquid water is almost continuously structured so as to promote complexation of two  $\text{H}_2\text{O}$  molecules, we set the pre-exponential factors of these reactions equal to  $k_B T/h$ .

## 2.4 Details of the cMD-DFT procedure

The cMD-DFT procedure is illustrated as a flowchart in Figure S8 in the ESI†.

### 2.4.1 Simulation boxes

Pt(111) catalysts were modeled using slabs comprised of three-layer 3 Pt  $\times$  3 Pt periodic surfaces (i.e., containing 27 total Pt atoms) in monoclinic  $p(3 \times 3)$  supercells with dimensions of  $a = b = 8.416 \text{ \AA}$  and angles of  $\alpha = \beta = 90.0^\circ$  and  $\gamma = 60.0^\circ$ . The (111) surface was created by cutting a slab from the structure of bulk Pt, which has a calculated lattice constant of  $3.967 \text{ \AA}$  (compared to the experimental value of  $3.924 \text{ \AA}$ <sup>76</sup>). Reaction intermediates and transition state (TS) complexes were added to the top surface layer. The total coverage of reaction intermediates or TSs

(not including liquid H<sub>2</sub>O molecules) was held constant at 1/9 monolayer (ML), where 1 ML is equal to 1 reaction intermediate or TS per surface metal atom. Liquid water was simulated by including up to 24 H<sub>2</sub>O molecules above the top Pt(111) surface layers. Configurations of these H<sub>2</sub>O molecules around reaction intermediates and TS complexes were obtained as follows. First, reaction intermediates and TS complexes geometries were obtained following the procedures described in Section 2.4.2. Since reaction intermediates and TS complexes could contain one or two H<sub>2</sub>O molecules, additional H<sub>2</sub>O molecules were added to the supercells so that the total number of H<sub>2</sub>O molecules in each supercell were equal to 24. The trajectories of all of the H<sub>2</sub>O molecules that were added to the supercells were simulated in cMD (Section 2.4.3), while the geometries of the reaction intermediates and TS complexes (including any involved H<sub>2</sub>O molecules) and Pt atoms were held fixed. In cMD simulations, the supercell *c* dimension was equal to 24.524 Å, giving a total supercell volume of 1505 Å<sup>3</sup> and a bulk water density of ~ 1 g/cm<sup>3</sup>. Configurations of H<sub>2</sub>O molecules were selected from the cMD trajectory and then partially re-optimized in DFT (Section 2.4.4). In DFT calculations, an additional 14 Å of vacuum space were added above the top of the liquid H<sub>2</sub>O structure, yielding a total *c* dimension of 38.524 Å, to minimize interactions between neighboring periodic images. Since only small perturbations were made to the liquid water structure in the DFT calculations (see Section 2.4.4), this addition had a negligible effect on the water density local to the reaction intermediates.

#### 2.4.2 Geometries of reaction intermediates and transition state complexes for use in cMD

Geometries of reaction intermediates for use in cMD were obtained using geometry relaxations performed in DFT under vacuum, and geometries of TS complexes for use in cMD were obtained in DFT under configurations of liquid H<sub>2</sub>O molecules (see Section 2.4.4), with the exceptions of the H<sub>2</sub>O and H<sub>5</sub>O<sub>2</sub> reaction intermediates and the TS complexes for the H<sub>2</sub>O-assisted COH\* dehydrogenation and H<sub>5</sub>O<sub>2</sub> dehydrogenation reactions (reactions (5) and (10)), which were generated from AIMD trajectories. These simulations were initiated from configurations sampled from cMD trajectories<sup>60</sup> and were performed in the canonical (NVT) ensemble at 300 K, maintained with the Nosé-Hoover thermostat.<sup>77,78</sup> Two total AIMD simulations were performed, one on a solvated COH\* species, and one on a solvated H<sub>5</sub>O<sub>2</sub> species. During the AIMD trajectories, the COH\* and H<sub>5</sub>O<sub>2</sub> species were observed to dehydrogenate to CO\* + H<sub>5</sub>O<sub>2</sub> and 2H<sub>2</sub>O + H\*, respectively. TS structures for use in cMD were taken from the respective times in the AIMD trajectories. Geometries of the H<sub>2</sub>O and H<sub>5</sub>O<sub>2</sub> reaction intermediates were generated from the trajectory of the solvated H<sub>5</sub>O<sub>2</sub> species. Further details about the AIMD simulations are provided in Section S4 the ESI†.

#### 2.4.3 Classical MD simulations

cMD simulations were performed in the NVT ensemble using the Large-scale Atomic/Molecular Massively Parallel Simulator (LAMMPS).<sup>79</sup> The target temperature was set to 300 K, which was maintained with the Nosé-Hoover thermostat.<sup>77,78</sup>

The timestep was 1 fs, and atomic positions were reported every 100 fs. Intermolecular energies were calculated with Lennard-Jones + Coulomb (LJ + C) potentials. LJ parameters for Pt atoms were taken from the universal force field (UFF)<sup>80</sup> and partial charges on Pt atoms were set to zero. LJ and C parameters for reaction intermediates were taken from the Optimized Potentials for Liquid Simulations (OPLS-AA)<sup>81</sup> force field, while those for water were taken from the Transferable Intermolecular Potential with 3 Points-Chemistry at Harvard Macromolecular Mechanics<sup>82</sup> (TIP3P-CHARMM) force field. Cross-terms for the LJ interactions were calculated using Lorentz-Berthelot mixing rules.<sup>83,84</sup> This model of H<sub>2</sub>O interactions with the catalytic surface is discussed further in Section S5 of the ESI†, including comparison with more detailed models. Water molecules were simulated as flexible in our cMD simulations, with bond and angle force constants and equilibrium bond lengths and angles taken from the TIP3P-CHARMM force field.<sup>82</sup> The cMD simulations were carried out for a total of 5 ns, where the first 2 ns were used for system equilibration and the remaining time was used to generate configurations of liquid H<sub>2</sub>O molecules. Configurations of liquid H<sub>2</sub>O molecules were selected at time intervals of at least 300 ps during the last 3 ns of the cMD runs. The 300 ps time interval was chosen because it is significantly longer than the longest “lifetime” of a hydrogen bond formed between a liquid H<sub>2</sub>O molecule and a reaction intermediates (110 ps, for the COH\* intermediate<sup>85</sup>).<sup>60</sup>

#### 2.4.4 DFT calculations

DFT calculations were performed using the Vienna Ab initio Simulation Package (VASP),<sup>86–89</sup> which employs planewave basis sets and periodic boundary conditions. Energies of core electrons were modeled using projector augmented-wave (PAW) pseudopotentials<sup>90,91</sup> to a cut-off energy of 400 eV, and exchange and correlation of valence electrons were modeled using the Perdew-Burke-Ernzerhof (PBE) functional.<sup>92,93</sup> The D2 dispersion correction<sup>94</sup> was used to improve the modeling of dispersion. Gaussian smearing with a smearing factor of 0.1 eV was used to set the partial occupancies of each orbital. The first Brillouin zones were sampled using automatically-generated 7 × 7 × 1 Monkhorst-Pack  $\Gamma$ -centered *k*-point meshes.<sup>95</sup> Electronic structures were converged self-consistently until the difference in energy between subsequent iterations was no larger than 10<sup>-5</sup> eV. Geometry relaxations for catalytic intermediates were performed using a force-based quasi-Newton algorithm.<sup>96</sup> In geometry relaxations performed under vacuum (for use in cMD), the reaction intermediates was allowed to relax, while all Pt atoms were held fixed. In geometry relaxations performed under configurations of liquid water (which were generated in cMD), geometries of any H<sub>2</sub>O molecules that were hydrogen bonded to the reaction intermediates were allowed to relax, while the geometries of the reaction intermediates, all other H<sub>2</sub>O molecules, and all Pt atoms were held fixed. Test simulations indicated that different relaxation strategies influenced interaction energies by < 0.1 eV. More information about the relaxation strategies tested is included in Section of S7 the ESI†. TS searches were performed using a combination of the climbing image-nudged elastic band<sup>97,98</sup> (CI-NEB) and dimer<sup>99</sup> methods under configurations of liquid H<sub>2</sub>O gener-

ated in cMD. Further details about how the configurations were generated are provided in Section S9 of the ESI†. CI-NEB simulations were performed using seven discrete images along the reaction coordinate (the initial and final images plus five intermediate images) connected with “springs” with force constants equal to  $5 \text{ eV}/\text{\AA}^2$ . The five intermediate images were relaxed in CI-NEB toward the minimum energy path (MEP) until the maximum force on all non-fixed atoms in all directions other than the reaction coordinate fell below  $0.5 \text{ eV}/\text{\AA}$ . A guess of the TS geometry was then generated from the resulting images using the neb2dim.pl script from Henkelman’s website,<sup>100</sup> and this structure was relaxed to a first order saddle point using the dimer method.<sup>99</sup> The convergence criterion for all geometry relaxations and transition state searches reported herein was that the maximum force on all of the non-fixed atoms be less than or equal to  $0.03 \text{ eV}/\text{\AA}$ . The structures of all TS complexes reported in this work were verified using vibrational mode analysis (details provided in Section S9 of the ESI†).

### 3 Results

#### 3.1 Structures and interaction energies of reaction intermediates

Calculated structures of  $\text{COH}^*$ ,  $\text{CO}^*$ ,  $\text{CH}_3\text{OH}^*$ ,  $\text{CH}_2\text{OH}^*$ ,  $\text{H}_2\text{O}$ ,  $\text{H}_5\text{O}_2^+$ ,  $\text{COH-H}_2\text{O}^*$ ,  $\text{COH-H}_2\text{O-H}_2\text{O}^*$ ,  $\text{CH}_3\text{OH-H}_2\text{O}^*$ , and  $\text{CH}_3\text{OH-H}_2\text{O-H}_2\text{O}^*$  are shown in Figure 1, and calculated values of  $\Delta E_{\text{int}}$  are given in Table 1. Further,  $\Delta E_{\text{int}}$  are compared with implicit solvation in Section S1.1 of the ESI†. Interaction energies are all negative (except for  $\text{H}^*$ , for which  $\Delta E_{\text{int}}$  is 0), indicating favorable interaction with liquid  $\text{H}_2\text{O}$ . Values range from  $-0.03 \pm 0.03 \text{ eV}$  for  $\text{CO}^*$  to  $-1.50 \pm 0.31 \text{ eV}$  for  $\text{H}_5\text{O}_2^+$ . The catalytic species with hydroxyl groups (all except  $\text{CO}^*$  and  $\text{H}^*$ ) have larger (more negative) interaction energies. For example, the interaction energy of  $\text{COH}^*$  (Figure 1a) is  $-0.70 \text{ eV}$ , meaning that the interaction with  $\text{H}_2\text{O}$  stabilizes  $\text{COH}^*$  on the Pt surface by  $-0.70 \text{ eV}$ . Further,  $\Delta E_{\text{int}}$  are stronger for species where the hydroxyl groups are sterically accessible to the liquid  $\text{H}_2\text{O}$  environment. For example, the  $\Delta E_{\text{int}}$  for  $\text{CH}_2\text{OH}^*$  (Figure 1d) is stronger at  $-0.65 \pm 0.12$  than for  $\text{CH}_3\text{OH}^*$  (Figure 1c) at  $-0.48 \pm 0.18$  because the  $-\text{OH}$  group on  $\text{CH}_2\text{OH}^*$  points up into the liquid  $\text{H}_2\text{O}$  environment, whereas the  $-\text{OH}$  group on  $\text{CH}_3\text{OH}^*$  points toward the Pt(111) surface. Similar comparisons can be made for  $\text{H}_5\text{O}_2^+$  (Figure 1f) versus  $\text{H}_2\text{O}$  (Figure 1e),  $\text{CH}_3\text{OH-H}_2\text{O}^*$  (Figure 1i) versus  $\text{COH-H}_2\text{O}^*$  (Figure 1g), and  $\text{CH}_3\text{OH-H}_2\text{O-H}_2\text{O}^*$  (Figure 1j) versus  $\text{COH-H}_2\text{O-H}_2\text{O}^*$  (Figure 1h).

#### 3.2 Calculated reaction energies

Calculated reaction energies are reported in Table 2 and plotted in Figure 2. They include contributions from the energy due to the breaking and forming of chemical bonds ( $\Delta E_{\text{rxn}}^{\text{vac}}$ ) as well as from the change in the water-adsorbate interaction ( $\Delta \Delta E_{\text{int}}$ ). Reactions where the aqueous environment stabilizes the reactant state more than the product state have a positive  $\Delta \Delta E_{\text{int}}$  and are therefore less thermodynamically favorable than their vacuum-phase analogues. Reactions (1) (i.e.,  $\text{COH}^* + * \rightarrow \text{CO}^* + \text{H}^*$ ), (2) (i.e.,  $\text{COH}^* + \text{H}_2\text{O} \rightarrow \text{COH-H}_2\text{O}^*$ ), (3) (i.e.,  $\text{COH-H}_2\text{O}^* +$

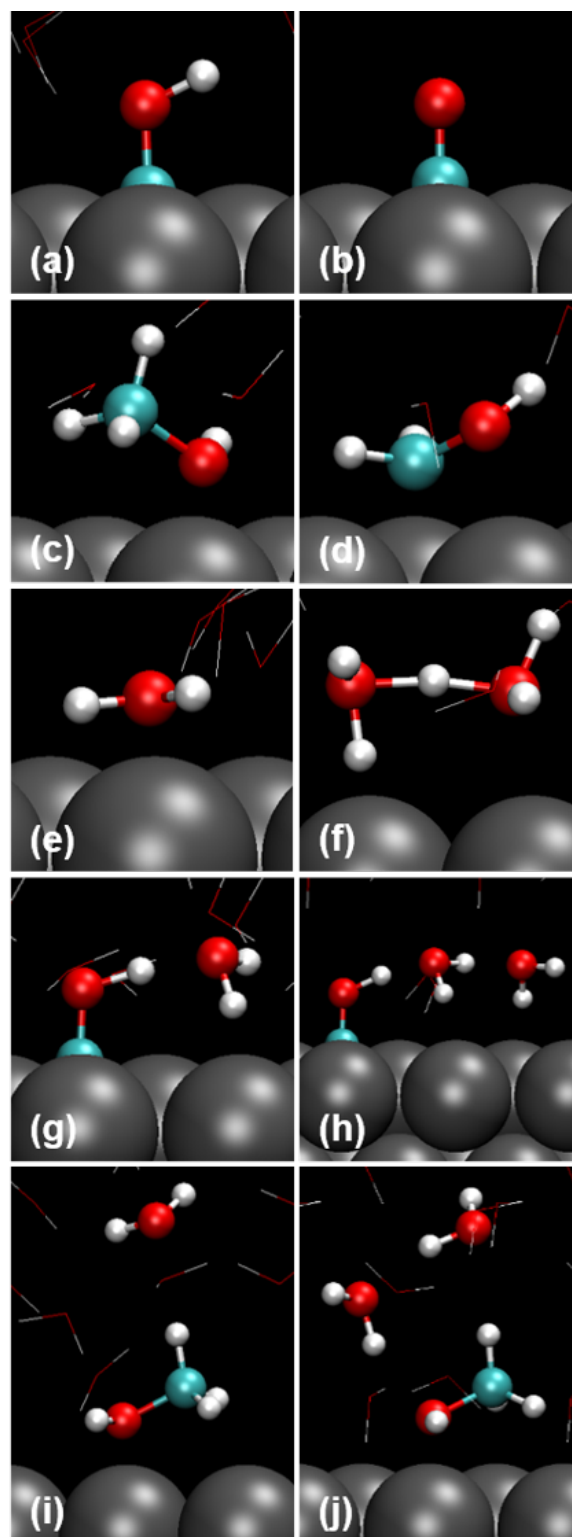


**Fig. 1** Geometries of (a)  $\text{COH}^*$ , (b)  $\text{CO}^*$ , (c)  $\text{CH}_3\text{OH}^*$ , (d)  $\text{CH}_2\text{OH}^*$ , (e)  $\text{H}_2\text{O}$ , (f)  $\text{H}_5\text{O}_2^+$ , (g)  $\text{COH-H}_2\text{O}^*$ , (h)  $\text{COH-H}_2\text{O-H}_2\text{O}^*$ , (i)  $\text{CH}_3\text{OH-H}_2\text{O-H}_2\text{O}^*$ , and (j)  $\text{H}^*$  on Pt(111) under liquid  $\text{H}_2\text{O}$ . Liquid water molecules are drawn as lines for visual clarity. Gray = Pt, teal = C, red = O, and white = H.

**Table 1** Calculated interaction energies in units of eV.

Reaction Intermediate or TS	$\Delta E_{\text{int}}$ [eV]
COH*	$-0.70 \pm 0.07$
CO*	$-0.03 \pm 0.03$
COH-H <sub>2</sub> O*	$-0.55 \pm 0.09$
COH-H <sub>2</sub> O-H <sub>2</sub> O*	$-1.07 \pm 0.17$
CH <sub>3</sub> OH*	$-0.48 \pm 0.18$
CH <sub>2</sub> OH*	$-0.64 \pm 0.12$
CH <sub>3</sub> OH-H <sub>2</sub> O*	$-1.29 \pm 0.20$
CH <sub>3</sub> OH-H <sub>2</sub> O-H <sub>2</sub> O*	$-1.27 \pm 0.29$
H*	$0.00 \pm 0.00$
* (vacant Pt site)	0 <sup>a</sup>
H <sub>2</sub> O	$-0.28 \pm 0.10$
H <sub>5</sub> O <sub>2</sub>	$-1.50 \pm 0.31$
TS, reaction 1	$-0.01 \pm 0.16$
TS, reaction 3	$-0.64 \pm 0.10$
TS, reaction 5	$-1.12 \pm 0.08$
TS, reaction 6	$-0.58 \pm 0.15$
TS, reaction 9	$-0.89 \pm 0.18$
TS, reaction 10	$-0.74 \pm 0.21$

<sup>a</sup> This value is 0 by definition.

\*  $\rightarrow$  CO\* + H\* + H<sub>2</sub>O), (8) (i.e., CH<sub>3</sub>OH-H<sub>2</sub>O\* + H<sub>2</sub>O  $\rightarrow$  CH<sub>3</sub>OH-H<sub>2</sub>O-H<sub>2</sub>O\*), and (10) (i.e., H<sub>5</sub>O<sub>2</sub> + \*  $\rightarrow$  2H<sub>2</sub>O + H\*) fall into this category. Conversely, reactions where the water environment stabilizes the product state more than the reactant state have a negative  $\Delta\Delta E_{\text{int}}$  and are therefore more thermodynamically favorable than their vacuum-phase analogs. Reactions (4) (i.e., COH-H<sub>2</sub>O\* + H<sub>2</sub>O  $\rightarrow$  COH-H<sub>2</sub>O-H<sub>2</sub>O\*), (5) (i.e., COH-H<sub>2</sub>O-H<sub>2</sub>O\*  $\rightarrow$  CO\* + H<sub>5</sub>O<sub>2</sub>), (6) (i.e., CH<sub>3</sub>OH\* + \*  $\rightarrow$  CH<sub>2</sub>OH\* + H\*), (7) (i.e., CH<sub>3</sub>OH\* + H<sub>2</sub>O  $\rightarrow$  CH<sub>3</sub>OH-H<sub>2</sub>O\*), and (9) (i.e., CH<sub>3</sub>OH-H<sub>2</sub>O-H<sub>2</sub>O\*  $\rightarrow$  CH<sub>2</sub>OH\* + H<sub>5</sub>O<sub>2</sub>) fall into this category. The magnitudes of  $\Delta\Delta E_{\text{int}}$  are significant at  $> 0.25$  eV for reactions (1), (2), (5), (7), (8), (9), and (10), indicating significant influence of the liquid H<sub>2</sub>O environment on the energies of these reactions. Further,  $\Delta E_{\text{rxn}}^{\text{vac}}$  and  $\Delta\Delta E_{\text{int}}$  directly counteract each other for reactions (1), (2), (3), (5), (7), (8), (9), and (10). Of these, the sign on  $\Delta E_{\text{rxn}}^{\text{aq}}$  is opposite of that on  $\Delta E_{\text{rxn}}^{\text{vac}}$  for all but reaction (2), indicating the ability of the liquid H<sub>2</sub>O environment to alter the energetic favorabilities of these reactions.

### 3.3 Transition states and activation energies

Calculated TS structures are shown in Figure 4, and activation barriers are reported in Table 2 and plotted in Figure 3. For reactions (1), (5), (6), and (10), the H<sub>2</sub>O environment has a similar influence on  $\Delta E_{\text{act}}^{\text{aq}}$  via  $\Delta\Delta E_{\text{int}}$  as for  $\Delta E_{\text{act}}^{\text{vac}}$ , whereas it has an opposite influence for reactions (2) and (9).  $\Delta\Delta E_{\text{int}}$  for reactions (1), (9), and (10) are positive, meaning that  $\Delta E_{\text{act}}^{\text{aq}} > \Delta E_{\text{act}}^{\text{vac}}$ , while  $\Delta\Delta E_{\text{int}}$  for reactions (3), (5), and (6) are negative, meaning that  $\Delta E_{\text{act}}^{\text{aq}} < \Delta E_{\text{act}}^{\text{vac}}$ . The magnitudes of  $\Delta\Delta E_{\text{int}}$  are significant at  $> 0.25$  eV for reactions (1), (9), and (10), indicating that the liquid H<sub>2</sub>O environment significantly influences the kinetics of these reactions.

Two of the activation barriers plotted in Figure 3 are negative.

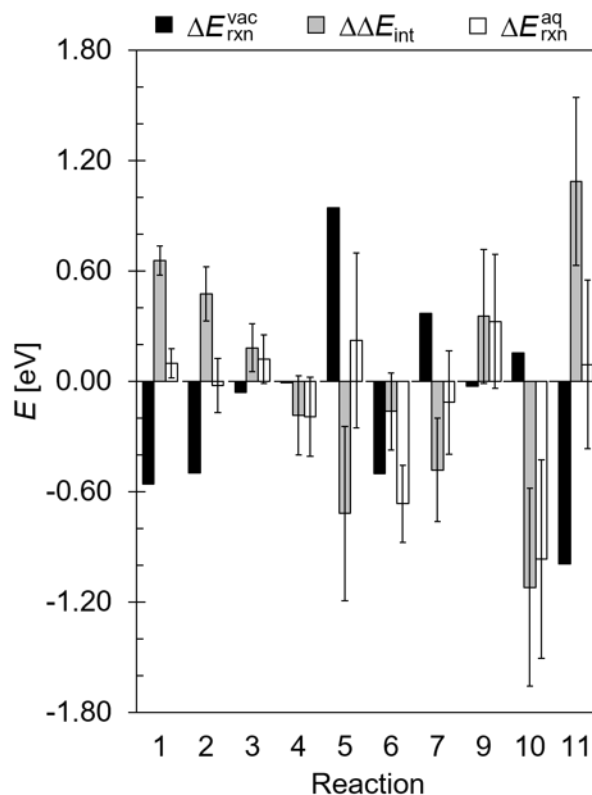


**Fig. 2** Calculated  $\Delta E_{\text{rxn}}^{\text{vac}}$  (black bars),  $\Delta\Delta E_{\text{int}}$  (gray bars), and  $\Delta E_{\text{rxn}}^{\text{aq}}$  (white bars) in units of eV.

$\Delta E_{\text{act}}^{\text{aq}}$  for reaction (3) is negative because  $\Delta E_{\text{act}}^{\text{vac}}$  for this reaction is  $\sim 0$  and  $\Delta\Delta E_{\text{int}}$  is  $\sim -0.10$  eV; however, the average value of  $\Delta E_{\text{act}}^{\text{aq}}$  is within the 95% confidence interval on  $\Delta\Delta E_{\text{int}}$ . For reaction (10), the TS complex was calculated to be lower in energy than the reactants in vacuum phase, suggesting that in vacuum phase, this reaction is not activated. In aqueous phase,  $\Delta E_{\text{act}}^{\text{aq}}$  for reaction (10) is positive (albeit small).

### 3.4 Pre-exponential factors

Calculated pre-exponential factors,  $A$ , are reported in Table 2. For reactions where we assumed the pre-exponential factor is  $k_B T/h$ ,  $A = 10^{12} \text{ s}^{-1}$  at the simulated temperature of 300 K. Reactions (2) and (7), i.e., where a liquid H<sub>2</sub>O molecule forms a complex with a COH\* or CH<sub>3</sub>OH\* species, require the liquid H<sub>2</sub>O structure to assume particular orientations. Since some orientations can promote co-catalyzed dehydrogenations, where the complexed H<sub>2</sub>O molecule abstracts a hydrogen from COH\* or CH<sub>3</sub>OH\* and simultaneously deposits a second hydrogen on the Pt(111) surface, we report two frequency factors for each of the complexation reactions in Table 2, one where the specific orientation could promote the co-catalyzed reaction (denoted “a” in Table 2) and one that generally describes the frequency of complexation and could promote co-catalyzed dehydrogenation or assisted dehydrogenation (denoted “b” in Table 2).

As the COH\* species is highly hydrophilic (i.e., having a  $\Delta E_{\text{int}}$  of  $-0.70$  eV), H<sub>2</sub>O molecules frequently orient so as to complex with



**Table 2** Calculated reaction energies ( $\Delta E_{\text{rxn}}^{\text{aq}}$ ), activation energies ( $\Delta E_{\text{act}}^{\text{aq}}$ ), and pre-exponential factors ( $A_{\text{for}}$ ).

No.	Reaction <sup>i</sup>	$\Delta E_{\text{rxn}}^{\text{aq}}$ [eV]	$\Delta E_{\text{act}}^{\text{aq}}$ [eV]	$A_{\text{for}}$ [ $s^{-1}$ ]
1	$\text{COH}^* + * \longrightarrow \text{CO}^* + \text{H}^*$	$0.10 \pm 0.08$	$1.68 \pm 0.18$	$6.25 \times 10^{12}$
2a	$\text{COH}^* + \text{H}_2\text{O} \longrightarrow \text{COH}-\text{H}_2\text{O}^*(\text{d})$	$-0.02 \pm 0.15$	ii	$(1.43 \pm 0.21) \times 10^{10}$
2b	$\text{COH}^* + \text{H}_2\text{O} \longrightarrow \text{COH}-\text{H}_2\text{O}^*$	"	ii	$(4.04 \pm 0.03) \times 10^{12}$
3	$\text{COH}-\text{H}_2\text{O}^*(\text{d}) + * \longrightarrow \text{CO}^* + \text{H}^* + \text{H}_2\text{O}$	$0.12 \pm 0.13$	$-0.09 \pm 0.13$	$6.25 \times 10^{12}$
4	$\text{COH}-\text{H}_2\text{O}^* + \text{H}_2\text{O} \longrightarrow \text{COH}-\text{H}_2\text{O}-\text{H}_2\text{O}^*$	$-0.19 \pm 0.22$	ii	$6.25 \times 10^{12}$
5	$\text{COH}-\text{H}_2\text{O}-\text{H}_2\text{O}^* \longrightarrow \text{CO}^* + \text{H}_5\text{O}_2$	$0.22 \pm 0.47$	$0.07 \pm 0.19$	$6.25 \times 10^{12}$
6	$\text{CH}_3\text{OH}^* + * \longrightarrow \text{CH}_2\text{OH}^* + \text{H}^*$	$-0.67 \pm 0.21$	$0.34 \pm 0.23$	$6.25 \times 10^{12}$
7a	$\text{CH}_3\text{OH}^* + \text{H}_2\text{O} \longrightarrow \text{CH}_3\text{OH}-\text{H}_2\text{O}^*(\text{d})$	$-0.11 \pm 0.28$	ii	$(3.00 \pm 1.24) \times 10^8$
7b	$\text{CH}_3\text{OH}^* + \text{H}_2\text{O} \longrightarrow \text{CH}_3\text{OH}-\text{H}_2\text{O}^*$	"	ii	$(6.87 \pm 0.70) \times 10^9$
8	$\text{CH}_3\text{OH}-\text{H}_2\text{O}^* + \text{H}_2\text{O} \longrightarrow \text{CH}_3\text{OH}-\text{H}_2\text{O}-\text{H}_2\text{O}^*$	$0.33 \pm 0.36$	ii	$6.25 \times 10^{12}$
9	$\text{CH}_3\text{OH}-\text{H}_2\text{O}-\text{H}_2\text{O}^* \longrightarrow \text{CH}_2\text{OH}^* + \text{H}_5\text{O}_2$	$-0.97 \pm 0.52$	$1.23 \pm 0.34$	$6.25 \times 10^{12}$
10	$\text{H}_5\text{O}_2 + * \longrightarrow 2\text{H}_2\text{O} + \text{H}^*$	$0.09 \pm 0.46$	$0.07 \pm 0.49$	$6.25 \times 10^{12}$

<sup>i</sup> (d) denotes the complex has a dangling hydrogen atom.

<sup>ii</sup> Did not calculate.

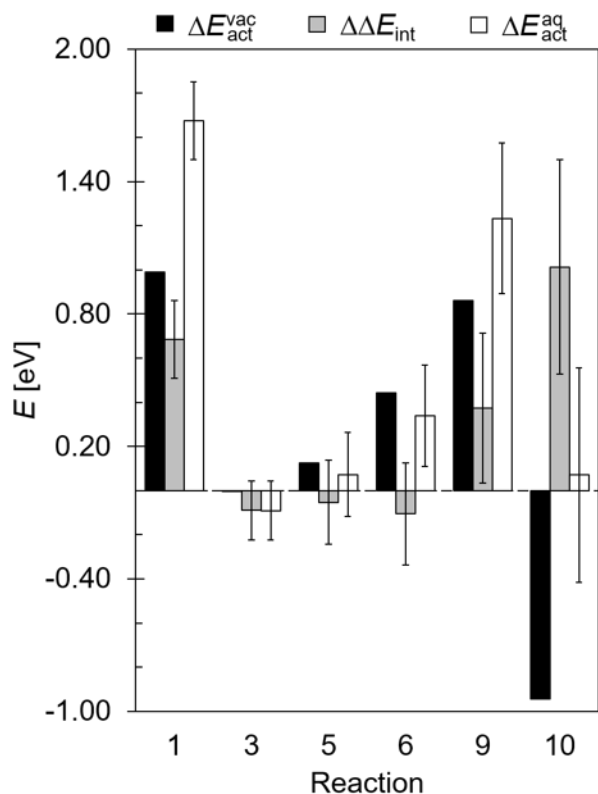


**Fig. 3** Calculated  $\Delta E_{\text{act}}^{\text{vac}}$  (black bars),  $\Delta\Delta E_{\text{int}}$  (gray bars), and  $\Delta E_{\text{act}}^{\text{aq}}$  (white bars) in units of eV.

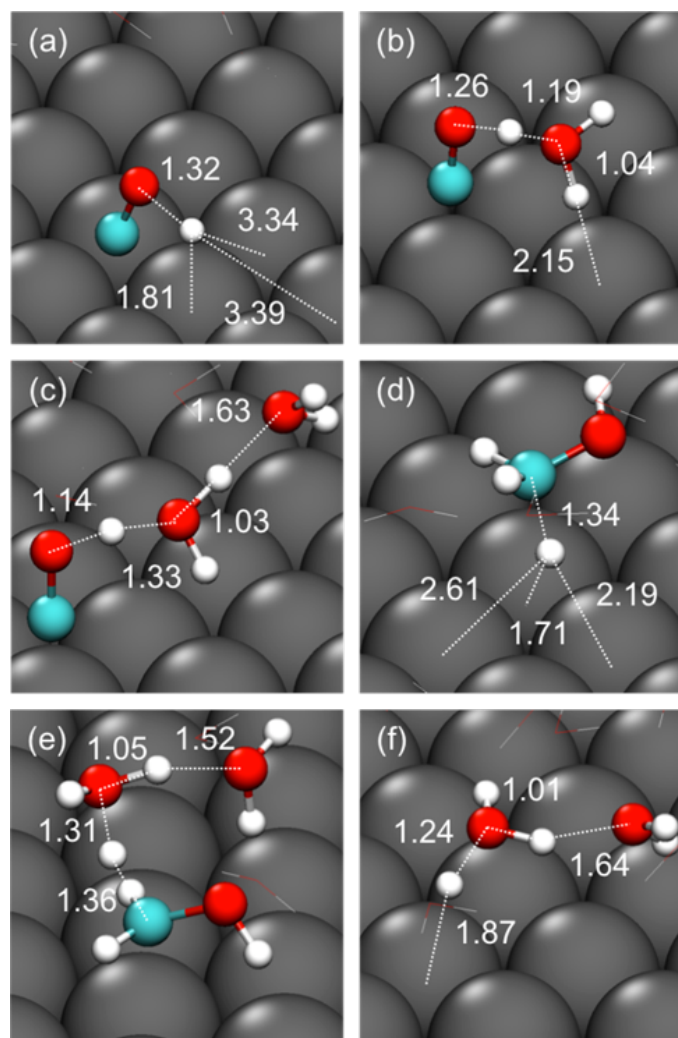


**Fig. 4** Representative TS structures for (a) reaction 1, (b) reaction 3, (c) reaction 5, (d) reaction 6, (e) reaction 9, and (f) reaction 10. Water molecules not involved in the TS complex are displayed as lines for visual clarity. Gray = Pt, teal = C, red = O, and white = H.



it; thus, the frequency of complexation between  $\text{COH}^*$  and liquid  $\text{H}_2\text{O}$  is high, on the order of  $10^{12} \text{ s}^{-1}$ . The large pre-exponential factor for this reaction suggests that  $\text{H}_2\text{O}$ -mediated  $\text{COH}^*$  dehydrogenation to  $\text{CO}^*$  is feasible. As orientations that could promote the co-catalyzed pathway require that the complexed  $\text{H}_2\text{O}$  molecule have a dangling hydrogen atom, which is a specific case, the frequency of forming these complexes is smaller, on the order of  $10^{10} \text{ s}^{-1}$ . According to Table 2,  $\sim 0.4\%$  of the  $\text{COH}-\text{H}_2\text{O}^*$  complexes that form could promote  $\text{H}_2\text{O}$ -co-catalyzed dehydrogenation.

$\text{CH}_3\text{OH}^*$  also interacts strongly with  $\text{H}_2\text{O}$ , with  $\Delta E_{\text{int}} = -0.48 \text{ eV}$ . However, this strong interaction energy is due to  $\text{H}_2\text{O}$  interactions with  $\text{CH}_3\text{OH}^*$ 's  $-\text{OH}$  group, whereas in this manuscript, we are interested in the chemistry that occurs at the  $-\text{CH}$  group. The  $-\text{CH}$  group interacts significantly less favorably with  $\text{H}_2\text{O}$ , evidenced by the remarkably small pre-exponential factor for forming  $\text{CH}_3\text{OH}-\text{H}_2\text{O}^*$  complexes at the  $-\text{CH}$  group, which is on the order of  $10^9 \text{ s}^{-1}$ . The special case that could promote  $\text{H}_2\text{O}$ -co-catalyzed  $\text{CH}_3\text{OH}^*$  dehydrogenation to  $\text{CH}_2\text{OH}^*$  is even smaller, representing only  $\sim 4\%$  of the total complexes that form at  $\text{CH}_3\text{OH}^*$ 's  $-\text{CH}$  group. Given that these pre-exponential factors are several orders of magnitude smaller than their non- $\text{H}_2\text{O}$ -mediated analogs,  $\text{CH}_3\text{OH}^*$  dehydrogenation to  $\text{CH}_2\text{OH}^*$  likely occurs via the direct pathway.

## 4 Discussion

Taking the results from Sections 3.2, 3.3, and 3.4 together, the liquid  $\text{H}_2\text{O}$  environment inhibits the direct dehydrogenation of  $\text{COH}^*$  (reaction (1), i.e.,  $\text{COH}^* + * \longrightarrow \text{CO}^* + \text{H}^*$ ). There are thermodynamic and kinetic penalties associated with breaking the  $\text{O}-\text{H}$  bond, since this results in a significantly weaker interaction with  $\text{H}_2\text{O}$ . In fact,  $\Delta E_{\text{act}}^{\text{aq}}$  for this reaction is prohibitively high in liquid  $\text{H}_2\text{O}$ . In contrast,  $\Delta E_{\text{act}}^{\text{aq}}$  for  $\text{H}_2\text{O}$ -mediated  $\text{COH}^*$  dehydrogenation are all  $< 0.25 \text{ eV}$ . Further, the pre-exponential factor for  $\text{H}_2\text{O}$ -mediated  $\text{COH}^*$  dehydrogenation is competitive to that for the direct dehydrogenation reaction. Thus,  $\text{COH}^*$  dehydrogenation to  $\text{CO}^*$  in liquid  $\text{H}_2\text{O}$  likely occurs through a  $\text{H}_2\text{O}$ -mediated pathway. The liquid  $\text{H}_2\text{O}$  environment thus has a significant influence on the pathway for  $\text{COH}^*$  dehydrogenation. In contrast, the liquid  $\text{H}_2\text{O}$  environment has a minor influence on the pathway for dehydrogenation of  $\text{CH}_3\text{OH}^*$  to  $\text{CH}_2\text{OH}^*$  (reaction (6) i.e.,  $\text{CH}_3\text{OH}^* + * \longrightarrow \text{CH}_2\text{OH}^* + \text{H}^*$ ).  $\Delta E_{\text{act}}^{\text{aq}}$  for this reaction is significantly smaller at  $0.34 \text{ eV}$  than that for  $\text{H}_2\text{O}$ -mediated  $\text{CH}_3\text{OH}^*$  dehydrogenation at  $1.23 \text{ eV}$ . Further, the frequencies of forming complexes that could lead to the  $\text{H}_2\text{O}$ -mediated  $\text{CH}_3\text{OH}^*$  dehydrogenation to  $\text{CH}_2\text{OH}^*$  are significantly smaller at  $10^9 \text{ s}^{-1}$  than those for the direct dehydrogenation reaction at  $10^{12} \text{ s}^{-1}$ . Hence,  $\text{CH}_3\text{OH}^*$  dehydrogenation to  $\text{CH}_2\text{OH}^*$  likely occurs through the direct pathway. These results are in agreement with isotopic labeling studies that have shown that water plays a role in catalytic  $\text{O}-\text{H}$  cleavage reactions but not  $\text{C}-\text{H}$  cleavage reactions.<sup>53</sup>

## 5 Conclusions

In this work, we used multiscale sampling to calculate reaction energies, activation energies, and pre-exponential factors for di-

rect and  $\text{H}_2\text{O}$ -mediated dehydrogenation of  $\text{COH}^*$  to  $\text{CO}^*$  and  $\text{CH}_3\text{OH}^*$  to  $\text{CH}_2\text{OH}^*$ . We find that  $\text{O}-\text{H}$  cleavage is thermodynamically and kinetically inhibited in the aqueous phase compared to in vacuum. In fact, the direct dehydrogenation reaction becomes kinetically implausible, having an activation barrier of  $1.7 \text{ eV}$ . As the  $-\text{OH}$  group interacts favorably with  $\text{H}_2\text{O}$ , the  $\text{O}-\text{H}$  cleavage reaction can occur via a  $\text{H}_2\text{O}$ -mediated pathway. We find that the activation barrier for  $\text{COH}^*$  dehydrogenation to  $\text{CO}^*$  is  $< 0.25 \text{ eV}$  and that the pre-exponential term is high, on the order of  $10^{12} \text{ s}^{-1}$ .  $\text{COH}^*$  dehydrogenation to  $\text{CO}^*$  thus likely proceeds via a  $\text{H}_2\text{O}$ -mediated pathway. The liquid  $\text{H}_2\text{O}$  environment thus has a strong influence on  $\text{COH}^*$  dehydrogenation to  $\text{CO}^*$ , inhibiting the energetics of the direct pathway so significantly that the reaction proceeds via a  $\text{H}_2\text{O}$ -mediated route. In contrast,  $\text{H}_2\text{O}$  influences on  $\text{C}-\text{H}$  cleavage are much more minor. The  $\text{H}_2\text{O}$ -mediated pathway for this reaction is not competitive, having an activation barrier  $> 1.0 \text{ eV}$  and a pre-exponential factor that is three orders of magnitude smaller than the direct pathway. The  $\text{H}_2\text{O}$  environment thus does not directly participate in  $\text{CH}_3\text{OH}^*$  dehydrogenation to  $\text{CH}_2\text{OH}^*$  and instead only serves to provide energetic alterations. In this case, the  $\text{H}_2\text{O}$  environment improves both the reaction energy and the activation energy of the direct  $\text{CH}_3\text{OH}^*$  to  $\text{CH}_2\text{OH}^*$  reaction.

## Conflicts of Interest

There are no conflicts to declare.

## Acknowledgements

This research was funded by the National Science Foundation through award number CBET-1438325. C.J.B. gratefully acknowledges fellowship support through NASA Training Grant NNX14AN43H. The authors also thank the Cyberinfrastructure Technology Integration (CITI) group at Clemson University for computational resources on the Palmetto Supercomputer Cluster.

## References

- 1 L. C. Grabow, in *Computational Catalysis*, ed. A. Asthagiri and M. J. Janik, The Royal Society of Chemistry, 2014, pp. 1–57.
- 2 J. K. Nørskov, T. Bligaard, J. Rossmeisl and C. H. Christensen, *Nat. Chem.*, 2009, **1**, 37–46.
- 3 G. W. Huber, S. Iborra and A. Corma, *Chem. Rev.*, 2006, **106**, 4044–4098.
- 4 R. R. Davda, J. W. Shabaker, G. W. Huber, R. D. Cortright and J. A. Dumesic, *Appl. Catal., B*, 2005, **56**, 171–186.
- 5 G. W. Huber and J. A. Dumesic, *Catal. Today*, 2006, **111**, 119–132.
- 6 G. Pipitone, D. Tosches, S. Bensaid, A. Galia and R. Pirone, *Catal. Today*, 2018, **304**, 153–164.
- 7 A. Hamnett, *Catal. Today*, 2016, **38**, 445–457.
- 8 A. S. Arico, S. Srinivasan and V. Antonucci, *Fuel Cells*, 2001, **1**, 133–161.
- 9 H. Liu, C. Song, L. Zhang, J. Zhang, H. Wang and D. P. Wilkinson, *J. Power Sources*, 2006, **155**, 95–110.
- 10 J. Greeley and M. Mavrikakis, *Nat. Mater.*, 2004, **3**, 810–815.

- 11 X. Li and A. Faghri, *J. Power Sources*, 2013, **226**, 223 – 240.
- 12 J. Xuan, M. K. Leung, D. Y. Leung and M. Ni, *Renewable Sustainable Energy Rev.*, 2009, **13**, 1301 – 1313.
- 13 B. P. Chaplin, M. Reinhard, W. F. Schneider, C. Schüth, J. R. Shapley, T. J. Strathmann and C. J. Werth, *Environ. Sci. Technol.*, 2012, **46**, 3655–3670.
- 14 N. Barrabés and J. Sá, *Appl. Catal. B*, 2011, **104**, 1–5.
- 15 K. Kabra, R. Chaudhary and R. L. Sawhney, *Ind. Eng. Chem. Res.*, 2004, **43**, 7683–7696.
- 16 S. Ahmed, M. Rasul, W. N. Martens, R. Brown and M. Hashib, *Desalination*, 2010, **261**, 3 – 18.
- 17 M. Pelaez, N. T. Nolan, S. C. Pillai, M. K. Seery, P. Falaras, A. G. Kontos, P. S. Dunlop, J. W. Hamilton, J. Byrne, K. O’Shea, M. H. Entezari and D. D. Dionysiou, *Appl. Catal., B*, 2012, **125**, 331 – 349.
- 18 C. Li, X. Zhao, A. Wang, G. W. Huber and T. Zhang, *Chem. Rev.*, 2015, **115**, 11559–11624.
- 19 C.-R. Chang, Z.-Q. Huang and J. Li, *Wiley Interdiscip. Rev.: Comput. Mol. Sci.*, 2016, **6**, 679–693.
- 20 D. D. Hibbitts, B. T. Loveless, M. Neurock and E. Iglesia, *Angew. Chem., Int. Ed.*, 2013, **52**, 12273–12278.
- 21 V. Polshettiwar and R. S. Varma, *Green Chem.*, 2010, **12**, 743–754.
- 22 S. D. Ebbesen, B. L. Mojét and L. Lefferts, *J. Catal.*, 2007, **246**, 66 – 73.
- 23 C. J. Bodenschatz, S. Sarupria and R. B. Getman, *J. Phys. Chem. C*, 2015, **119**, 13642–13651.
- 24 Y. Okamoto, O. Sugino, Y. Mochizuki, T. Ikeshoji and Y. Morikawa, *Chem. Phys. Lett.*, 2003, **377**, 236–242.
- 25 D. Skachkov, C. Venkateswara Rao and Y. Ishikawa, *J. Phys. Chem. C*, 2013, **117**, 25451–25466.
- 26 S. Desai and M. Neurock, *Electrochim. Acta*, 2003, **48**, 3759 – 3773.
- 27 C. Hartnig and E. Spohr, *Chem. Phys.*, 2005, **319**, 185–191.
- 28 J. Liu, X.-M. Cao and P. Hu, *Phys. Chem. Chem. Phys.*, 2014, **16**, 4176–4185.
- 29 C. Michel, J. Zaffran, A. M. Ruppert, J. Matras-Michalska, M. Jędrzejczyk, J. Grams and P. Sautet, *Chem. Commun.*, 2014, **50**, 12450–12453.
- 30 C. Hartnig, J. Grimming and E. Spohr, *J. Electroanal. Chem.*, 2007, **607**, 133–139.
- 31 Z.-Q. Huang, B. Long and C.-R. Chang, *Catal. Sci. Technol.*, 2015, **5**, 2935–2944.
- 32 C. Hartnig, J. Grimming and E. Spohr, *Electrochim. Acta*, 2007, **52**, 2236–2243.
- 33 J. K. Nørskov, J. Rossmeisl, A. Logadottir, L. Lindqvist, J. R. Kitchin, T. Bligaard and H. Jonsson, *J. Phys. Chem. B*, 2004, **108**, 17886–17892.
- 34 R. Jinnouchi, K. Kodama and Y. Morimoto, *J. Electroanal. Chem.*, 2014, **716**, 31 – 44.
- 35 S. T. Dix, J. K. Scott, R. B. Getman and C. T. Campbell, *Faraday Discuss.*, 2016, **188**, 21–38.
- 36 M. Faheem, S. Suthirakun and A. Heyden, *J. Phys. Chem. C*, 2012, **116**, 22458–22462.
- 37 N. Artrith and A. M. Kolpak, *Nano Lett.*, 2014, **14**, 2670–2676.
- 38 M. Neurock, S. A. Wasileski and D. Mei, *Chem. Eng. Sci.*, 2004, **59**, 4703–4714.
- 39 J. A. Santana, C. R. Cabrera and Y. Ishikawa, *Phys. Chem. Chem. Phys.*, 2010, **12**, 9526–9534.
- 40 J. A. Herron, Y. M. Morikawa and M. Mavrikakis, *PNAS*, 2016, E4937–E4945.
- 41 H.-F. Wang and Z.-P. Liu, *J. Phys. Chem. C*, 2009, **113**, 17502–17508.
- 42 T. Xie, S. Sarupria and R. B. Getman, *Mol. Sim.*, 2017, **43**, 370–378.
- 43 T. Xie, C. J. Bodenschatz and R. B. Getman, *React. Chem. Eng.*, 2019, **4**, 383–392.
- 44 L. Bellarosa, R. García-Muelas, G. Revilla-López and N. López, *ACS Cent. Sci.*, 2016, **2**, 109–116.
- 45 X. Nie, W. Luo, M. Janik and A. Asthagiri, *J. Catal.*, 2014, **312**, 108–122.
- 46 M. J. Janik and M. Neurock, *Electrochim. Acta*, 2007, **52**, 5517–5528.
- 47 J. A. Santana, J. J. Mateo and Y. Ishikawa, *J. Phys. Chem. C*, 2010, **114**, 4995–5002.
- 48 J. A. Santana, J. J. Saavedra-Arias and Y. Ishikawa, *Electrocatalysis*, 2015, **6**, 534–543.
- 49 S. Behtash, J. Lu, M. Faheem and A. Heyden, *Green Chem.*, 2014, **16**, 605–616.
- 50 C. Michel and P. Gallezot, *ACS Catal.*, 2015, **5**, 4130–4132.
- 51 D. Cao, G.-Q. Lu, A. Wieckowski, S. A. Wasileski and M. Neurock, *J. Phys. Chem. B*, 2005, **109**, 11622–11633.
- 52 M. P. Hyman and J. W. Medlin, *J. Phys. Chem. B*, 2006, **110**, 15338–15344.
- 53 M. B. Boucher, M. D. Marcinkowski, M. L. Liriano, C. J. Murphy, E. A. Lewis, A. D. Jewell, M. F. G. Mattera, G. Kyriakou, M. Flytzani-Stephanopoulos and E. C. H. Sykes, *ACS Nano*, 2013, **7**, 6181–6187.
- 54 L. R. Merte, G. Peng, R. Bechstein, F. Rieboldt, C. A. Farberow, L. C. Grabow, W. Kudernatsch, S. Wendt, E. Lægsgaard, M. Mavrikakis and F. Besenbacher, *Science*, 2012, **336**, 889–893.
- 55 J. Saavedra, H. A. Doan, C. J. Pursell, L. C. Grabow and B. D. Chandler, *Science*, 2014, **345**, 1599–1602.
- 56 X. Zhang, T. E. Sewell, B. Glatz, S. Sarupria and R. B. Getman, *Catal. Today*, 2017, **285**, 57–64.
- 57 L. Árnadóttir, E. M. Stuve and H. Jónsson, *Chem. Phys. Lett.*, 2012, **541**, 32–38.
- 58 S. K. Desai, V. Pallassana and M. Neurock, *J. Phys. Chem. B*, 2001, **105**, 9171–9182.
- 59 A. J. R. Hensley, Y. Wang, D. Mei and J.-S. McEwen, *ACS Catal.*, 2018, **8**, 2200–2208.
- 60 C. J. Bodenschatz, X. Zhang, T. Xie, J. Arvay, S. Sarupria and R. B. Getman, *J. Visualized Exp.*, 2019, **In Press**.
- 61 A. C. Van Duin, S. Dasgupta, F. Lorant and W. A. Goddard, *J. Phys. Chem. A*, 2001, **105**, 9396–9409.

- 62 Y. Wu, H. Chen, F. Wang, F. Paesani and G. A. Voth, *J. Phys. Chem. B*, 2008, **112**, 467–482.
- 63 Y. Han, D. Jiang, J. Zhang, W. Li, Z. Gan and J. Gu, *Front. Chem. Sci. Eng.*, 2016, **10**, 16–38.
- 64 A. Savara, I. Rossetti, C. E. Chan-Thaw, L. Prati and A. Villa, *ChemCatChem*, 2016, **8**, 2482–2491.
- 65 J. Greeley and M. Mavrikakis, *J. Am. Chem. Soc.*, 2004, **126**, 3910–3919.
- 66 H. Ogasawara, B. Brena, D. Nordlund, M. Nyberg, A. Pel-menschikov, L. Pettersson and A. Nilsson, *Physical review let-ters*, 2002, **89**, 276102.
- 67 G. Zimbitas, S. Haq and A. Hodgson, *The Journal of chemical physics*, 2005, **123**, 174701.
- 68 S. Haq, J. Harnett and A. Hodgson, *Surface science*, 2002, **505**, 171–182.
- 69 G. A. Kimmel, N. G. Petrik, Z. Dohnálek and B. D. Kay, *The Journal of chemical physics*, 2006, **125**, 044713.
- 70 M. J. Janik, C. D. Taylor and M. Neurock, *Top. Catal.*, 2007, **46**, 306–319.
- 71 Z. Cao, R. Kumar, Y. Peng and G. A. Voth, *The Journal of Physical Chemistry C*, 2015, **119**, 14675–14682.
- 72 J.-S. Filhol and M.-L. Doublet, *Catalysis today*, 2013, **202**, 87–97.
- 73 E. S. Stoyanov, I. V. Stoyanova and C. A. Reed, *J. Am. Chem. Soc.*, 2010, **132**, 1484–1485.
- 74 A. Luzar and D. Chandler, *Nature*, 1996, **379**, 55–57.
- 75 J. Teixeira and M.-C. Bellissent-Funel, *J. Phys.: Condens. Matter*, 1990, **2**, SA105.
- 76 D. R. Lide, *CRC Handbook of Chemistry and Physics*, CRC Press Boca Raton, FL, 1997, vol. 78.
- 77 S. Nosé, *Mol. Phys.*, 1984, **52**, 255–268.
- 78 W. G. Hoover, *Phys. Rev. A*, 1985, **31**, 1695–1697.
- 79 S. Plimpton, *J. Comput. Phys.*, 1995, **117**, 1–19.
- 80 A. K. Rappé, C. J. Casewit, K. Colwell, W. Goddard Iii and W. Skiff, *J. Am. Chem. Soc.*, 1992, **114**, 10024–10035.
- 81 K. Kahn and T. C. Bruice, *J. Comput. Chem.*, 2002, **23**, 977–996.
- 82 A. D. MacKerell, D. Bashford, M. Bellott, R. Dunbrack, J. D. Evanseck, M. J. Field, S. Fischer, J. Gao, H. Guo, S. Ha *et al.*, *J. Phys. Chem. B*, 1998, **102**, 3586–3616.
- 83 H. Lorentz, *Ann. Phys.*, 1881, **248**, 127–136.
- 84 D. Berthelot, *Comptes Rendus*, 1898, **126**, 1703–1706.
- 85 X. Zhang, R. S. DeFever, S. Sarupria and R. B. Getman, *J. Chem. Inf. Model.*, 2019, **In Press**.
- 86 G. Kresse and J. Hafner, *Phys. Rev. B*, 1993, **47**, 558.
- 87 G. Kresse and J. Hafner, *Phys. Rev. B*, 1994, **49**, 14251.
- 88 G. Kresse and J. Furthmüller, *Comput. Mater. Sci.*, 1996, **6**, 15–50.
- 89 G. Kresse and J. Furthmüller, *Phys. Rev. B*, 1996, **54**, 11169.
- 90 P. E. Blöchl, *Phys. Rev. B*, 1994, **50**, 17953.
- 91 G. Kresse and D. Joubert, *Phys. Rev. B*, 1999, **59**, 1758.
- 92 J. P. Perdew, K. Burke and M. Ernzerhof, *Phys. Rev. Lett.*, 1996, **77**, 3865.
- 93 J. P. Perdew, K. Burke and M. Ernzerhof, *Phys. Rev. Lett.*, 1997, **78**, 1396.
- 94 S. Grimme, *J. Comput. Chem.*, 2006, **27**, 1787–1799.
- 95 H. J. Monkhorst and J. D. Pack, *Phys. Rev. B*, 1976, **13**, 5188.
- 96 P. Pulay, *Chem. Phys. Lett.*, 1980, **73**, 393–398.
- 97 G. Henkelman and H. Jonsson, *J. Chem. Phys.*, 2000, **113**, 9901–9904.
- 98 G. Henkelman and H. Jonsson, *J. Chem. Phys.*, 2000, **113**, 9978–9985.
- 99 G. Henkelman and H. Jonsson, *J. Chem. Phys.*, 1999, **111**, 7010.
- 100 G. Henkelman, *VASP TST Tools*, <http://theory.cm.utexas.edu/vtsttools/>, Accessed: 09-26-2017.

TOC Entry: Reaction energies and activation barriers for dehydrogenation reactions of methanol derivatives under realistic liquid water configurations using a multiscale method.

